Serb. Astron. J. № 185 (2012), 53 - 64 **UDC 524.722.7–77 : 524.523**
DOI: 10.2298/SAJ1285053W Professional paper

NEW 20-cm RADIO-CONTINUUM STUDY OF THE SMALL MAGELLANIC CLOUD: PART III – COMPACT H II REGIONS

G. F. Wong, M. D. Filipović, E. J. Crawford, N. F. H. Tothill, A. Y. De Horta and T. J. Galvin

University of Western Sydney, Locked Bag 1797, Penrith South DC, NSW 2751, Australia
E–mail: *m.filipovic@uws.edu.au*

(Received: October 29, 2012; Accepted: November 6, 2012)

SUMMARY: We present and discuss a new catalogue of 48 compact H II regions in the Small Magellanic Cloud (SMC) and a newly created deep 1420 MHz (λ=20 cm) radio-continuum image of the N 19 region located in the southwestern part of the SMC. The new images were created by merging 1420 MHz radio-continuum archival data from the Australian Telescope Compact Array. The majority of these detected radio compact H II regions have rather flat spectral indices which indicates, as expected, that the dominant emission mechanism is of thermal nature.

Key words. Magellanic Clouds – radio continuum: ISM – catalogs

1. INTRODUCTION

The Small Magellanic Cloud (SMC), with its well established distance (∼60 kpc; Hilditch et al. 2005) and ideal position in the sky - towards the coldest areas near the South Celestial Pole, allows observation of radio sources to be conducted without significant interference from Galactic foreground radiation. The SMC is an ideal location to study celestial objects like compact H II regions (Mezger et al. 1967), which may be difficult to study in our own and other distant galaxies.

The SMC has been surveyed at multiple radio frequencies using archival data (Crawford et al. 2011, Wong et al. 2011a, hereafter Paper I). Deep observations of SMC young stellar objects, compact H II regions, Supernova Remnants (SNRs) and Planetary Nebulae (PNe) were presented in Oliveira et al. (2012), Indebetouw et al. (2004), Filipović et al. (2005), Filipović et al. (2008) and Filipović et al. (2009), respectively. A catalogue of radio-continuum point sources (Wong et al. 2012) towards the SMC was derived from images taken from Crawford et al. (2011).

This is the third paper in this series; Paper I presented newly developed high sensitivity and resolution images of the SMC. The second instalment (Wong et al. 2011b, hereafter Paper II) presented a point source catalogue created from the images in paper I. In this paper, we present newly constructed images of the N 19 region covering the southwestern part of the SMC, at ν=1.4 GHz (λ=20 cm). We also present a catalogue of compact H II regions sources towards the SMC. The catalogue is derived from images at 4800 MHz (λ=6 cm) and 8600 MHz (λ=3 cm) from Crawford et al. (2011), a 2370 MHz ($\lambda = 13$ cm) mosaic image from Filipović et al. (2002), one of our SMC 20 cm mosaic radio-continuum images (Fig. 2 in Paper I), the N 19 images presented in this paper and an 843 MHz (λ=36 cm) MOST image (Turtle et al. 1998).

In Section 2 we describe the data used to create the N 19 images and identify the compact H II region. In Section 3 we describe our source fitting and detection methods. In Section 4 we present our new maps with a brief discussion, Section 5 contains our conclusions, and the Appendix contains the catalogue of compact H II regions.

2. DATA

2.1. SMC Mosaic Radio-continuum Images

The 3 and 6 cm images (Fig. 3 and Fig. 1 in Crawford et al. 2011) were created by combining data from various ATCA projects that covered the SMC (Table 1 in Crawford et al. 2011). The 3 and 6 cm maps have resolutions of $\sim$20″ and $\sim$30″ and r.m.s. noise of 0.8 and 0.7 mJy/beam, respectively. The 13 cm radio-continuum catalogue was produced from a SMC mosaic radio survey of 20 square degrees (Filipović et al. 2002). These observations have a beam size of $\sim$40″ and r.m.s. noise of 0.4 mJy/beam. The 20 cm mosaic image (Fig. 2 in Paper I) was created by combining data from ATCA project C1288 (Mao et al. 2008) with data obtained for a Parkes radio-continuum study of the SMC (Filipović et al. 1997). This image has a beam size of 17.″8 × 12.″2 with r.m.s. noise of 0.7 mJy/beam.

The 36 cm image comes from the MOST radio survey of 36 square degrees containing the SMC field (Turtle et al. 1998). These observations have a beam size of $\sim$45″ and r.m.s. noise of 0.7 mJy/beam — equal to that of the 20 cm image.

Table 1 gives the field size and central position of all images used to derive the compact H II region catalogue contained in this paper.

Table 1. Field size and central position of SMC images used.

Image	RA	Dec	Field Size
3 cm	01:00:00	-73:00:00	5°× 5°
6 cm	01:00:00	-73:00:00	5°× 5°
13 cm	01:00:00	-72:50:00	5°× 4°
20 cm	01:00:00	-72:00:30	7°× 9°
36 cm	01:00:00	-72:30:30	6°× 6°

2.2. The SMC N 77 region

Observations were conducted with ATCA (project C281) over two 12 hour sessions on August 25, 1993 and February 10, 1994. Two array configurations at 20 and 13 cm (ν=1377/2377 MHz) were used – 1.5B and 6B. More details about these observations can be found in Ye et al. (1995) and Bojičić et al. (2010).

2.3. The SMC N 19 region

2.3.1. Image Creation

In order to create high-fidelity and high-resolution radio-continuum images of the SMC N 19 region, we searched the Australia Telescope Online Archive[1] (ATOA), identifying three complementary ATCA observations that covered N 19: projects C468, C882 and C1607. The source 1934-638 was used as the primary calibrator and 0252-712 as the secondary calibrator for all ATCA SMC observations. A brief summary of the three ATCA projects is shown in Table 2.

The software packages MIRIAD (Sault and Killeen 2010) and KARMA (Gooch 2006) were used for the data reduction and analysis. Initial high-resolution images were produced from the full dataset using the MIRIAD multi-frequency synthesis (Sault and Wieringa 1994) with natural weighting. The deconvolution process used MIRIAD tasks MOSSDI, an SDI variant of the clean algorithm designed for mosaics (Steer et al. 1984).

Figs. 1-3 show maps from individual ATCA projects (Table 2), Figs. 4 and 5 show maps derived from combining multiple observations.

Table 2. ATOA data used to image N 19.

ATCA Project	Date Observed	Array
C468	1997 Aug 06–07	375
	1995 Oct 26–27	1.5D
	1997 Nov 22	6C
C882	2000 Jun 20–17	6B
C1607	2006 Dec 02–12	6B
	2006 Dec 12–18	750A

2.3.2. Images

Comparing individual maps of N 19 (Figs. 1–3), we can see the effects of different array configurations. Fig. 1 is created from project C468, containing a combination of extended and point source emission, as a result of three different array configurations. Fig. 2 (project C882) only contains a long-baseline observation (array configuration 6B), so the map is dominated by point sources. Fig. 3 has extended and point source emission, derived from short and long-baseline array configurations 750A and 6B respectively. Table 3 lists the details of the individual maps.

Table 3. Details of N 19 mosaics at 20-cm.

ATCA Project	Beam Size (arcsec)	Position Angle	r.m.s. noise (mJy/beam)
C468	5.3×5.1	2.°7	0.1
C882	6.6×6.2	-1.°3	0.1
C1607	6.9×5.5	-2.°8	0.1

[1] http://atoa.atnf.csiro.au

Figs. 4 and 5 show images created from a combination of observations (Table 2): Fig. 4 was created from ATCA projects C468 and C1607 while Fig. 5 contains observations C468, C882 and C1607. The images contain a combination of point sources and extended emission.

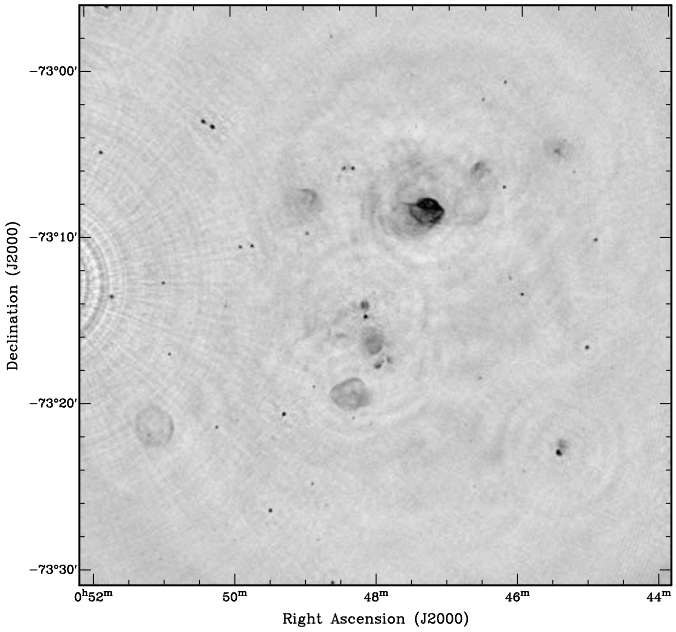

Fig. 1. *ATCA project C468 radio-continuum total intensity image of N 19. The synthesised beam is 5″.3×5″.1 and the r.m.s. noise is ∼0.1 mJy/beam.*

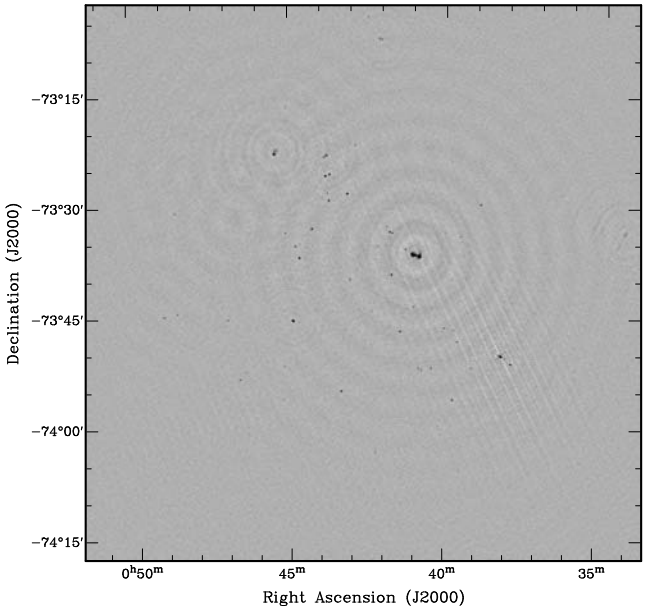

Fig. 2. *ATCA project C882 radio-continuum total intensity image of N 19. The synthesised beam is 6″.6×6″.2 and the r.m.s. noise is ∼0.1 mJy/beam.*

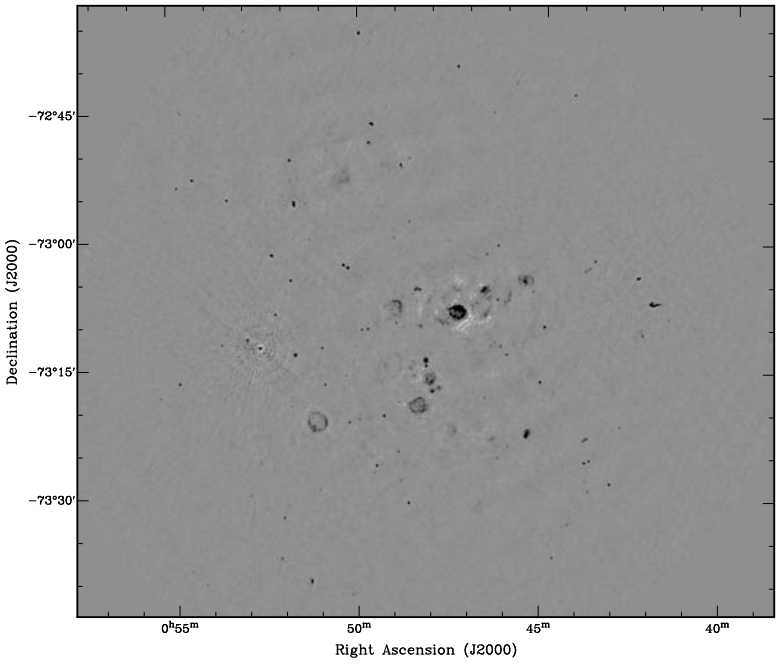

Fig. 3. *ATCA project C1607 radio-continuum total intensity image of N 19. The synthesised beam is 6″.9×5″.5 and the r.m.s. noise is ∼0.1 mJy/beam.*

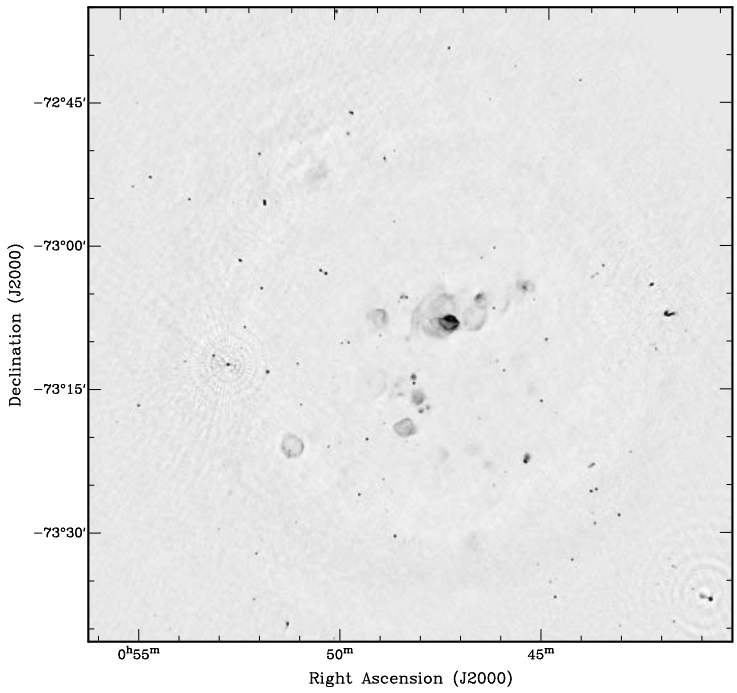

Fig. 4. *Combined ATCA projects C468 and C1607 radio-continuum total intensity image of N 19. The synthesised beam is 5″.3×5″.0 and the r.m.s. noise is ∼0.1 mJy/beam.*

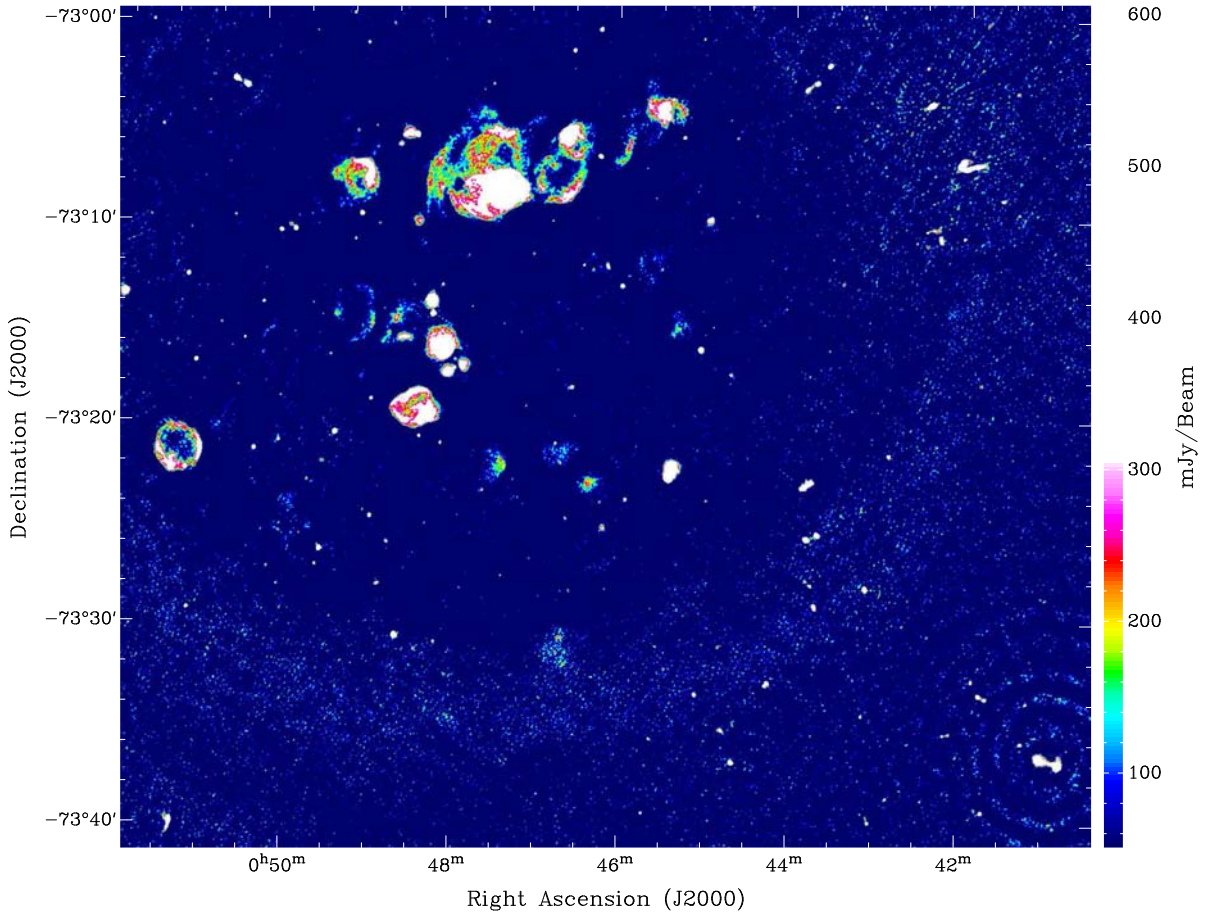

Fig. 5. *20 cm total intensity continuum image of N 19, derived from ATCA projects C468, C882 and C1607. The synthesised beam is 5.″3×5.″0 and the r.m.s. noise is ∼0.1 mJy/beam.*

3. THE SMC COMPACT H II REGIONS: SOURCE FITTING AND DETECTION

Compact H II regions were identified by comparing our list of radio-continuum point sources (Paper II and Wong et al. 2012) to an Hα observation from the Magellanic Cloud Emission Line Survey (MCELS; Smith et al. 1999). Sources were examined visually to confirm that matched Hα sources were point or point-like in Hα and within ∼5″of the radio point source detection.

The list of candidate compact H II regions was narrowed down by cross-checking with catalogues of known objects like supernova remnants (Filipović et al. 2008) and planetary nebulae (Filipović et al. 2009, Crawford et al. 2012, Bojičić et al. 2010).

Table A1 gives the names, positions (J2000, derived from the 1420 MHz image of the whole SMC) and the integrated flux values at various frequencies for the compact H II regions. The integrated fluxes in columns 5–12 are: flux density values taken from the MOST image; 1420 MHz flux density measurements from SMC (high resolution Fig. 2, Paper I) and new N 19 (Fig. 5) mosaic images; flux measurements retrieved from the N 77 20 and 13 cm images (Ye et al. 1995); flux values from an SMC 2370 MHz mosaic image (Filipović et al. 2002); 4800 and 8640 MHz flux values from Crawford et al. (2011; Figs. 1 and 3).

4. RESULTS AND DISCUSSION

Figs. 1–3 show the individual intensity mosaic maps of the N 19 region derived from projects C468, C882 and C1607, respectively, while Figs. 4 and 5 are images created by combining different observations. All these images can be downloaded from: space-science.uws.edu.au/mc/smc/N19/. A sample of 48 compact H II regions was selected; table A1 lists the compact H II regions with integrated flux values at various frequencies. These flux values are derived from gaussians fitted to the images described in Section 2.

30 of the 48 catalogue sources were detected at more than one wavelength. Spectral indices α ($S_\nu \propto \nu^\alpha$), with errors, were estimated for all of these sources, fitted to all available flux measurements. Integrated fluxes at 1 GHz were also derived from these fits. Integrating the fitted spectra from 10 MHz to 100 GHz yielded fluxes (in $10^{-26}\,\mathrm{W\,m^{-2}}$) which were then converted into radio luminosities using the known distance to the SMC. Table A2 lists all compact H II regions: The estimated flux density at 1 GHz; spectral index with errors; and the radio luminosity (i.e. the luminosity of the compact H II region over the radio spectrum) in units of 10^{26} W and in solar luminosities.

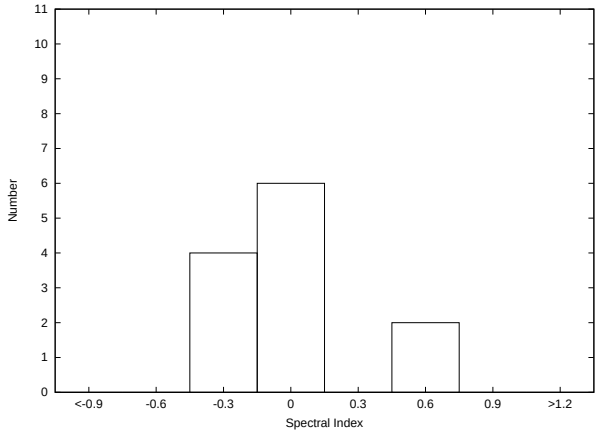

Fig. 6. *Spectral Index distribution of compact H II regions in N 19.*

Figs. 6–8 contain spectral index distributions of the compact H II regions in the N 19 region in the SMC (without N 19) and the combination of the two. We expect compact H II regions to have flat radio spectra ($\alpha \approx -0.1$), turning into $\alpha \approx 2$ below the cutoff frequency (which depends on the individual region); the spectral index distributions are indeed peaked around small values of α. While the spectral index distribution of SMC sources has a broad peak with several sources having quite large α, the distribution of N 19 sources is much more sharply peaked near $\alpha = 0$. The maps of N 19 have better resolution and sensitivity than the maps of the rest of the SMC, so the N 19 sources might be expected to have more accurate fluxes and hence more accurate spectral indices. Overall, ∼60% of the sources have spectral index within the expected range of $-0.3 < \alpha < 0.3$. Higher spectral indices may be explained by the cutoff frequency lying within the frequency range of our observations (see notes on individual sources below). There are also a few sources with significantly negative spectral indices, which is not consistent with thermal emission — these may be contaminating non-H II region sources.

The radio luminosity distribution (Fig. 9) peaks around $\sim 0.3\,\mathrm{L_\odot}$: It falls off towards higher luminosities as there are fewer sufficiently bright stars to power compact H II regions at such high luminosities; it falls off towards lower luminosities due to the lack of completeness of our catalogue. Our catalogue is likely to be quite complete down to a limiting radio luminosity of $\sim 0.3\,\mathrm{L_\odot}$.

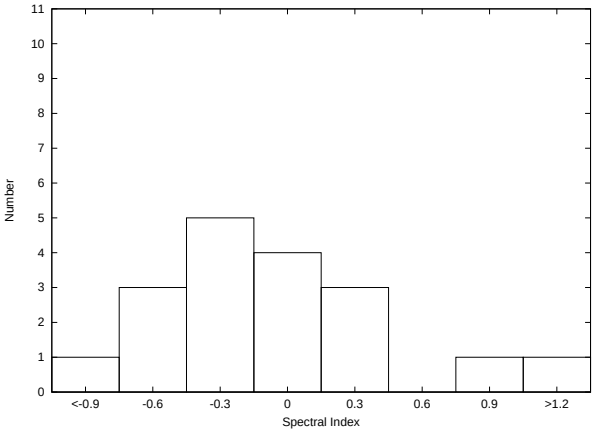

Fig. 7. *Spectral Index distribution of SMC compact H II regions (excluding N 19 sources).*

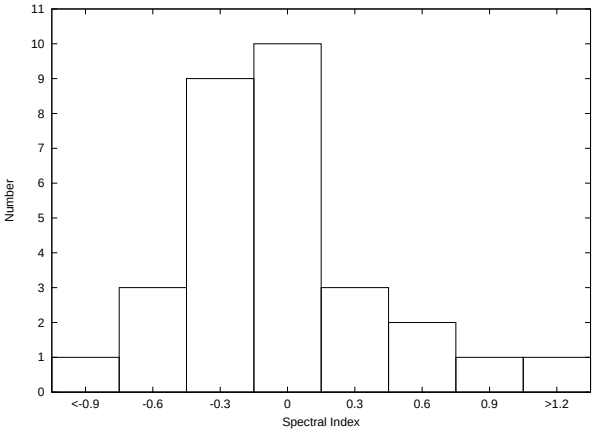

Fig. 8. *Spectral Index distribution of compact H II regions in SMC (including N 19 sources).*

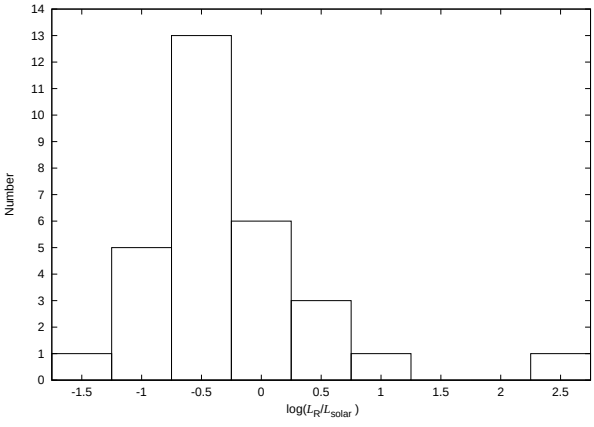

Fig. 9. *Radio luminosity distribution of SMC compact H II regions from all maps.*

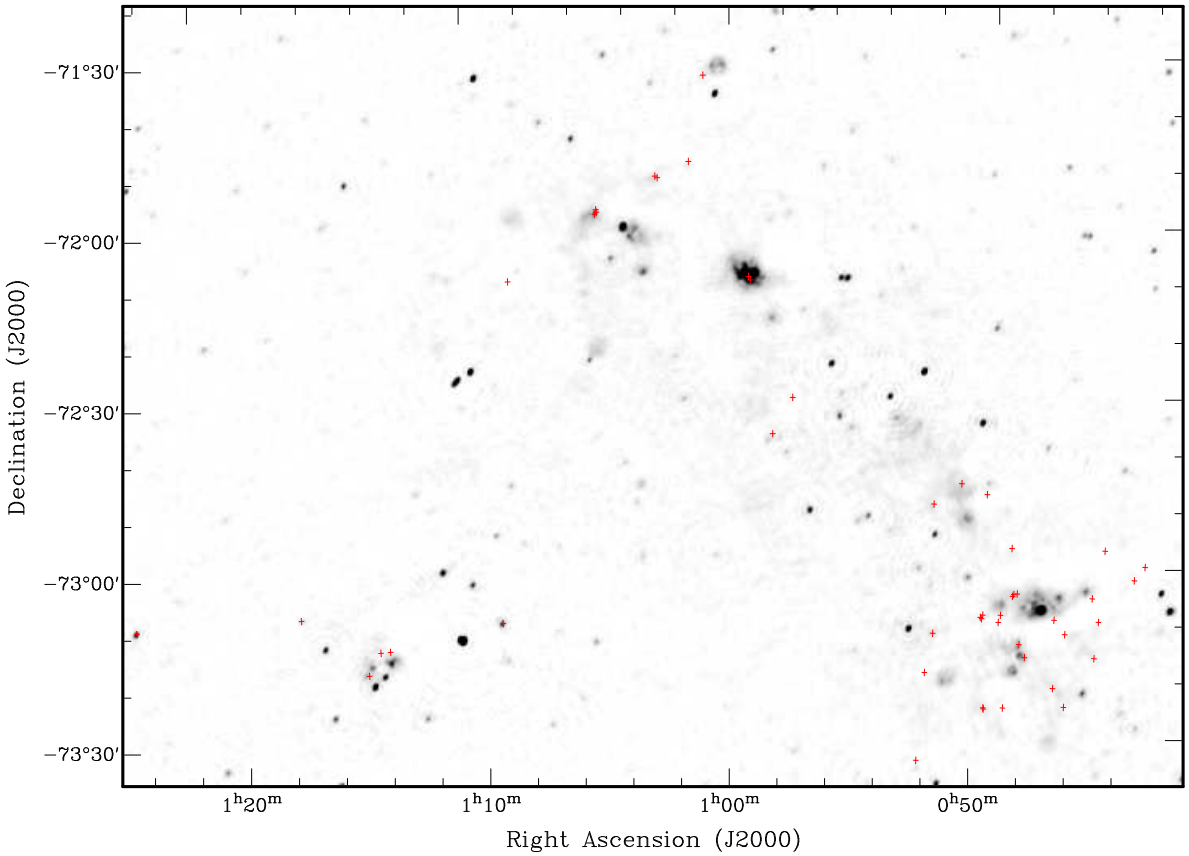

Fig. 10. *Location of compact H II regions overlaid on a continuum map of the SMC (Fig 6, Paper I).*

4.1. Notes on individual sources

4.1.1. J005914-721103 (Source 33)

This compact H II region candidate is the extreme positive outlier in Figs. 7 and 8, with a spectral index of $+2.0 \pm 0.4$; it is only detected in the 13 cm and 20 cm N 77 images, so the spectral index is defined purely by these fluxes. It is possible that this is a compact H II region with a very high-frequency spectral break, so that it has a spectral index of 2 even in the higher-frequency maps. However, in the 13 cm image, the source is located at the edge of the primary beam, so that the 13 cm flux is rather unreliable, and so this spectral index may not be accurate. It is also possible that this source could be a variable background galaxy that flared during the N 77 observations, and is otherwise undetected. The very high estimated luminosity is largely due to the extreme spectral index, and is unlikely to be accurate — if the source is indeed a compact H II region with a very high cutoff frequency, the high luminosity is due to extrapolation of the low-frequency spectral index to the whole radio region.

4.1.2. J010132-715042 (Source 36)

This is the other source with a highly positive spectral index ($+1.0 \pm 0.4$), and could only be detected in the 20 cm and 36 cm images. It is likely that this is a compact H II region whose spectral break lies between 36 cm and 20 cm. Fitting a single power-law to these data then gives an average spectral index of about 1. This will also lead to a large overestimate in the luminosity.

4.1.3. J012408-730904 (Source 48)

This compact H II region candidate has a very high radio luminosity of 23.5 $L_{\odot}$; this estimate comes from a combination of a positive estimated spectral index (which implies rising flux through the GHz spectrum, and hence a large luminosity) and very high fluxes in all images. The source is detected at 36 cm, and the higher-frequency data yield a spectral index of $\sim -0.2 \pm 0.1$. This is quite consistent with the source being a compact H II region with a cutoff

frequency between 843 MHz and 1.4 GHz. Although the luminosity may be overestimated, this is clearly a very luminous radio source. If it is a compact H II region, it is likely to be powered by a cluster of young high-mass stars, which can supply such a large luminosity.

5. CONCLUSION

In this paper we present a new catalogue of 48 candidate compact H II regions within the SMC. This catalogue is derived from previously-presented datasets, and from a new set of high-sensitivity and high-resolution radio-continuum images of the N 19 region at 1420 MHz (λ=20 cm), created from archival ATCA data. We have collected flux measurements at as many wavelengths as possible for all sources, and used these fluxes to fit a power-law radio spectrum, which, in turn, yields estimates of the flux at 1 GHz and the spectral index. The distribution of spectral indices is consistent with a population of sources dominated by compact H II regions, i.e. peaked around $\alpha \approx 0$, with better data yielding sharper peaks, and a few sources with significantly positive spectral indices — consistent with compact H II regions whose cutoff frequencies lie within our frequency range. We have also estimated the radio luminosity of the sources: The distribution of radio luminosities is strongly peaked around a presumed threshold luminosity, but includes some very luminous regions, such as J012408-730904, whose very high radio luminosity suggests that it is powered by a cluster of young high-mass stars.

Acknowledgements – The Australia Telescope Compact Array is part of the Australia Telescope National Facility which is funded by the Commonwealth of Australia for operation as a National Facility managed by CSIRO. This paper includes archived data obtained through the Australia Telescope Online Archive (http://atoa.atnf.csiro.au). We used the KARMA and MIRIAD software packages developed by ATNF. We thank the anonymous referee and Richard Sturm for their valuable comments, which have led to an improved paper.

REFERENCES

Bojičić, I. S., Filipović, M. D., Crawford, E. J.: 2010, *Serb. Astron. J.*, **181**, 63.

Dickel, J. R., Gruendl, R. A., McIntyre, V. J., Shaun, W. A.: 2010, *Astron. J.*, **140**, 1511.

Crawford, E. J., Filipović, M. D., de Horta, A. Y., Wong, G. F., Tothill, N. F. H., Drašković,, D., Collier, J. D., Galvin, T. J.: 2011, *Serb. Astron. J.*, **183**, 95.

Crawford, E. J., Filipović, M. D., Bojičić, I. S., Cohen, M., Payne, J. L., De Horta, A. Y., Reid, W.: 2012, *IAU Symposium Vol. 283 of IAU Symposium.*

Filipović, M. D., Jones, P. A., White, G. L, Haynes, R. F, Klein, U., Wielebinski, R.: 1997, *Astron. Astrophys. Suppl. Series*, **121**, 321.

Filipović, M. D., Haynes, R. F., White, G. L., Jones, P. A.: 1998, *Astron. Astrophys. Suppl. Series*, **130**, 421.

Filipović, M. D., Bohlsen, T., Reid, W, Staveley-Smith, L., Jones, P. A, Nohejl, K., Goldstein, G.: 2002, *Mon. Not. R. Astron. Soc.*, **335**, 1085.

Filipović, M. D., Payne, J. L., Reid, W., Danforth, C. W., Staveley-Smith, L., Jones, P. A., White, G. L.: 2005, *Mon. Not. R. Astron. Soc.*, **364**, 217.

Filipović, M. D., Haberl, F., Winkler, P. F., Pietsch, W., Payne, J. L., Crawford, E. J., de Horta, A. Y., Stootman, F. H., Reaser, B. E.: 2008, *Astron. Astrophys.*, **485**, 63.

Filipović, M. D., Cohen, M., Reid, W. A., Payne, J. L., Parker, Q. A., Crawford, E. J., Bojičić, I. S., de Horta, A. Y., Hughes, A., Dickel, J., Stootman, F.: 2009, *Mon. Not. R. Astron. Soc.*, **399**, 769.

Gooch, R.: 2008, KARMA Users Manual, ATNF, Sydney.

Hilditch, R. W., Howarth, I. D., Harries, T. J.: 2005, *Mon. Not. R. Astron. Soc.*, **357**, 304.

Indebetouw, R., Johnson, K. E., Conti, P.: 2004, *Astron. J.*, **128**, 2206.

Mao, S. A., Gaensler, B. M., Stanimirović, S., Haverkorn, M., McClure-Griffiths, N. M., Staveley-Smith, L., Dickey, J. M.: 2008, *Astrophys. J.*, **688**, 1029.

Mezger, P. G., Altenhoff, W., Schraml, J., Burke, B. F., Reifenstein, E. C., III, Wilson, T. L.: 1967, *Astron. J.*, **150**, L157.

Oliveira, J. M., Th. van Loon, J., Sloan, G. C., Sewilo, M., Kraemer, K.E.,Wood, P. R., Indebetouw, R., Filipović, M. D., Crawford, E. J., Wong, G. F., Hora, J. L., Meixner M., Robitaille, T. P., Shiao, B. Simon, J. D.: 2012, *Mon. Not. R. Astron. Soc.*, (in press).

Sault, R., Killeen, N.: 2010, Miriad Users Guide, ATNF.

Sault, R. J., Wieringa, M. H.: 1994, *Astron. Astrophys. Suppl. Series*, **108**, 585.

Smith,R. C. and MCELS Team: 1999, *IAU Symposium Vol. 190 of IAU Symposium.*

Steer, D. G., Dewdney, P. E., Ito, M. R.: 1984, *Astron. Astrophys.*, **137**, 159.

Turtle, A. J., Ye, T., Amy, S. W., Nicholls, J.: 1998, *Publ. Astron. Soc. Aust.*, **15**, 280.

Wong, G. F., Filipović, M. D., Crawford, E. J., de Horta, A. Y., Galvin, T., Drašković, D., Payne, J. L.: 2011a, *Serb. Astron. J.*, **182**, 43.

Wong, G. F., Filipović, M. D., Crawford, E. J., Tothill, N. F. H., de Horta, A. Y., Drašković, D., Galvin, T. J., Collier, J. D., Payne, J. L.: 2011b, *Serb. Astron. J.*, **183**, 103.

Wong, G. F., Crawford, E. J., Filipović, M. D., De Horta, A. Y., Tothill, N. F. H., Collier, J. D., Drašković, D., Galvin, T. J., Payne, J. L.: 2012, *Serb. Astron. J.*, **184**, 93.

Ye, T. S., Amy, S. W., Wang, Q. D., Ball, L., Dickel, J.: 1995, *Mon. Not. R. Astron. Soc.*, **275**, 1218.

APPENDIX

Table A1. Compact H II regions and their fluxes.

(1) No	(2) Name	(3) RA (J2000)	(4) Dec (J2000)	(5) S_{843} (mJy)	(6) S_{1420} (SMC) (mJy)	(7) S_{1420} (N 19) (mJy)	(8) S_{1377} (N77) (mJy)	(9) S_{2377} (N77) (mJy)	(10) S_{2370} (SMC) (mJy)	(11) S_{4800} (mJy)	(12) S_{8640} (mJy)
1	J004312-725958	00:43:12.6	-72:59:58	—	—	0.55	—	—	—	—	—
2	J004336-730227	00:43:36.4	-73:02:27	5.9	5.0	2.44	—	—	5.2	5.8	4.8
3	J004451-725734	00:44:51.6	-72:57:34	—	2.3	0.20	—	—	—	—	—
4	J004457-731012	00:44:57.1	-73:10:12	5.7	3.0	2.66	—	—	4.6	5.2	3.5
5	J004502-731639	00:45:02.6	-73:16:39	6.3	6.4	2.61	—	—	5.4	4.4	4.5
6	J004515-730607	00:45:15.7	-73:06:07	—	—	1.54	—	—	—	—	—
7	J004610-732534	00:46:10.7	-73:25:34	—	—	0.40	—	—	—	—	—
8	J004617-731243	00:46:17.7	-73:12:43	—	—	0.23	—	—	—	—	—
9	J004640-732221	00:46:40.3	-73:22:21	—	—	0.31	—	—	—	—	—
10	J004645-731017	00:46:45.9	-73:10:17	—	—	0.19	—	—	—	—	—
11	J004753-731709	00:47:53.5	-73:17:09	—	6.7	0.38	—	—	—	—	—
12	J004808-731454	00:48:08.6	-73:14:54	19.8	15.6	12.47	—	—	11.2	16.2	18.3
13	J004818-730558	00:48:18.7	-73:05:58	—	4.9	2.15	—	—	—	—	—
14	J004826-730606	00:48:27.0	-73:06:06	—	4.9	1.93	—	—	—	—	—
15	J004829-730626	00:48:29.9	-73:06:26	—	4.4	0.42	—	—	—	—	—
16	J004836-725759	00:48:36.4	-72:57:59	—	2.8	1.59	—	—	—	2.2	—
17	J004841-732614	00:48:41.8	-73:26:14	—	—	0.58	—	—	—	—	—
18	J004857-730952	00:48:57.1	-73:09:52	—	1.6	0.91	—	—	—	—	—
19	J004901-731109	00:49:01.8	-73:11:09	—	—	0.45	—	—	—	—	1.6
20	J004929-732633	00:49:29.2	-73:26:33	9.7	7.2	5.53	—	—	4.1	5.9	5.6
21	J004930-732621	00:49:30.4	-73:26:21	—	—	0.23	—	—	—	—	—
22	J004940-730958	00:49:40.4	-73:09:58	—	—	0.15	—	—	—	—	—
23	J004941-724840	00:49:41.5	-72:48:40	6.6	2.8	1.42	—	—	3.4	5.7	5.5
24	J004942-731037	00:49:42.7	-73:10:37	7.3	3.6	3.25	—	—	—	5.2	3.5
25	J004946-731024	00:49:46.1	-73:10:24	—	—	0.25	—	—	—	—	—
26	J005043-724655	00:50:43.4	-72:46:55	—	7.1	0.53	—	—	—	—	—
27	J005141-731331	00:51:41.2	-73:13:31	12.5	7.7	2.88	—	—	5.7	10.8	8.0
28	J005148-725041	00:51:48.3	-72:50:41	9.2	7.2	2.27	—	—	5.1	5.9	6.6
29	J005158-732030	00:51:58.3	-73:20:30	—	—	0.32	—	—	—	—	—
30	J005212-733604	00:52:12.6	-73:36:04	—	1.4	0.20	—	—	—	1.3	—

Table A1. Continued.

(1) No	(2) Name	(3) RA (J2000)	(4) Dec (J2000)	(5) S_{843} (mJy)	(6) S_{1420} (SMC) (mJy)	(7) S_{1420} (N 19) (mJy)	(8) S_{1377} (N77) (mJy)	(9) S_{2377} (N77) (mJy)	(10) S_{2370} (SMC) (mJy)	(11) S_{4800} (mJy)	(12) S_{8640} (mJy)
31	J005729-723223	00:57:29.9	-72:32:23	4.0	4.4	—	—	—	1.4	3.3	3.3
32	J005816-723849	00:58:16.5	-72:38:49	12.7	5.1	—	—	—	5.0	14.8	9.5
33	J005914-721103	00:59:14.9	-72:11:03	—	—	—	2.2	5.9	—	—	—
34	J005911-721140	00:59:11.0	-72:11:40	—	—	—	—	—	—	7.0∗	5.0∗
35	J010058-713527	01:00:58.5	-71:35:27	9.3	6.7	—	—	—	4.7	7.5	7.5
36	J010132-715042	01:01:32.2	-71:50:42	1.5	2.4	—	—	—	—	—	—
37	J010243-715331	01:02:43.6	-71:53:31	8.1	2.5	—	0.4	—	—	2.6	1.6
38	J010248-715314	01:02:48.7	-71:53:14	13.9	9.1	—	5.9	6.9	5.3	8.9	12.1
39	J010503-715926	01:05:03.8	-71:59:26	—	14.5	—	5.8	12.5	—	24.5	17.4
40	J010504-715900	01:05:05.0	-71:59:00	—	5.9	—	2.5	3.0	—	10.5	4.7
41	J010508-715946	01:05:08.4	-71:59:46	—	7.9	—	3.1	—	—	10.3	6.2
42	J010832-721119	01:08:32.4	-72:11:19	—	—	—	—	—	—	0.8∗	0.6∗
43	J010912-731138	01:09:13.0	-73:11:38	50.0	33.1	—	—	—	60.1	35.7	37.5
44	J011352-731546	01:13:52.1	-73:15:46	8.7	3.5	—	—	—	—	4.7	4.8
45	J011415-731550	01:14:15.8	-73:15:50	9.5	4.3	—	—	—	5.9	7.2	8.2
46	J011447-731946	01:14:47.1	-73:19:46	15.0	8.0	—	—	—	3.4	4.0	5.2
47	J011724-730917	01:17:25.0	-73:09:17	20.1	12.5	—	—	—	7.4	4.3	4.7
48	J012408-730904	01:24:08.1	-73:09:04	39.6	51.4	—	—	—	115.3	92.8	94.2

∗ Values taken from Indebetouw et al. 2004

Table A2. Compact H II regions and their properties.

(1) No	(2) Name	(3) RA (J2000)	(4) Dec (J2000)	(5) S_{1000} (mJy)	(6) Spectral Index	(7) Luminosity $\times 10^{26}$ W/Hz	(8) Luminosity in $L_\odot$
1	J004312-725958	00:43:12.6	-72:59:58	—	—	—	—
2	J004336-730227	00:43:36.4	-73:02:27	4.4	0.1 ± 0.2	2.5	0.6
3	J004451-725734	00:44:51.6	-72:57:34	—	—	—	—
4	J004457-731012	00:44:57.1	-73:10:12	4.0	0.0 ± 0.2	1.7	0.5
5	J004502-731639	00:45:02.6	-73:16:39	5.0	-0.1 ± 0.2	1.7	0.4
6	J004515-730607	00:45:15.7	-73:06:07	—	—	—	—
7	J004610-732534	00:46:10.7	-73:25:34	—	—	—	—
8	J004617-731243	00:46:17.7	-73:12:43	—	—	—	—
9	J004640-732221	00:46:40.3	-73:22:21	—	—	—	—
10	J004645-731017	00:46:45.9	-73:10:17	—	—	—	—
11	J004753-731709	00:47:53.5	-73:17:09	—	—	—	—
12	J004808-731454	00:48:08.6	-73:14:54	14.9	0.0 ± 0.1	7.1	1.9
13	J004818-730558	00:48:18.7	-73:05:58	—	—	—	—
14	J004826-730606	00:48:27.0	-73:06:06	—	—	—	—
15	J004829-730626	00:48:29.9	-73:06:26	—	—	—	—
16	J004836-725759	00:48:36.4	-72:57:59	2.1	0.1 ± 0.4	1.1	0.3
17	J004841-732614	00:48:41.8	-73:26:14	—	—	—	—
18	J004857-730952	00:48:57.1	-73:09:52	—	—	—	—
19	J004901-731109	00:49:01.8	-73:11:09	0.3	0.7 ± 0.1	2.2	0.6
20	J004929-732633	00:49:29.2	-73:26:33	7.0	-0.2 ± 0.1	1.7	0.4
21	J004930-732621	00:49:30.4	-73:26:21	—	—	—	—
22	J004940-730958	00:49:40.4	-73:09:58	—	—	—	—
23	J004941-724840	00:49:41.5	-72:48:40	3.1	0.2 ± 0.3	3.1	0.8
24	J004942-731037	00:49:42.7	-73:10:37	4.8	-0.1 ± 0.2	1.4	0.4
25	J004946-731024	00:49:46.1	-73:10:24	—	—	—	—
26	J005043-724655	00:50:43.4	-72:46:55	—	—	—	—
27	J005141-731331	00:51:41.2	-73:13:31	6.7	0.1 ± 0.3	3.9	1.0
28	J005148-725041	00:51:48.3	-72:50:41	5.5	0.0 ± 0.3	2.6	0.7
29	J005158-732030	00:51:58.3	-73:20:30	—	—	—	—
30	J005212-733604	00:52:12.6	-73:36:04	0.4	0.7 ± 1.4	2.8	0.7
31	J005729-723223	00:57:29.9	-72:32:23	3.3	-0.1 ± 0.3	1.1	0.3
32	J005816-723849	00:58:16.5	-72:38:49	7.7	0.1 ± 0.3	5.1	1.3
33	J005911-721140	00:59:11.0	-72:11:40	17.3	-0.6 ± 0.3	1.2	0.3
34	J005914-721103	00:59:14.9	-72:11:03	1.1	2.0 ± 0.4	1363.6	355.2
35	J010058-713527	01:00:58.5	-71:35:27	7.2	-0.0 ± 0.1	2.7	0.7
36	J010132-715042	01:01:32.2	-71:50:42	1.7	1.0 ± 0.4	35.4	9.2
37	J010243-715331	01:02:43.6	-71:53:31	2.4	-0.2 ± 0.7	0.5	0.1
38	J010248-715314	01:02:48.7	-71:53:14	8.1	0.0 ± 0.2	4.1	1.1
39	J010503-715926	01:05:03.8	-71:59:26	8.4	0.5 ± 0.3	20.2	5.3
40	J010504-715900	01:05:05.0	-71:59:00	3.4	0.3 ± 0.4	4.7	1.2
41	J010508-715946	01:05:08.4	-71:59:46	4.9	0.2 ± 0.4	5.0	1.3
42	J010832-721119	01:08:32.4	-72:11:19	1.7	-0.5 ± 0.3	0.1	0.0
43	J010912-731138	01:09:13.0	-73:11:38	46.1	-0.1 ± 0.1	14.2	3.7
44	J011352-731546	01:13:52.1	-73:15:46	5.9	-0.1 ± 0.2	1.5	0.4
45	J011415-731550	01:14:15.8	-73:15:50	6.5	0.1 ± 0.2	3.3	0.9
46	J011447-731946	01:14:47.1	-73:19:46	9.3	-0.5 ± 0.3	0.9	0.2
47	J011724-730917	01:17:25.0	-73:09:17	15.5	-0.7 ± 0.1	0.9	0.2
48	J012408-730904	01:24:08.1	-73:09:04	51.2	0.4 ± 0.2	90.0	23.4

НОВО ПРОУЧАВАЊЕ МАЛОГ МАГЕЛАНОВОГ ОБЛАКА У РАДИО-КОНТИНУУМУ НА 20 cm: ДЕО III - КОМПАКТНИ H II РЕГИОНИ

G. F. Wong, M. D. Filipović, E. J. Crawford, N. F. H. Tothill, A. Y. De Horta and T. J. Galvin

University of Western Sydney, Locked Bag 1797, Penrith South DC, NSW 2751, Australia

E–mail: *m.filipovic@uws.edu.au*

УДК 524.722.7–77 : 524.523

Стручни чланак

Представљамо нови каталог од 48 компактних H II региона у Малом Магелановом Облаку (ММО). Такође, представљамо и нове радио-континуум слике N19 региона који се налази у југозападном делу ММО. Нове слике су креиране спајањем свих расположивих 20 cm посматрања са ATCA телескопа (Australian Telescope Compact Array). Већина детектованих комапктних H II региона има типичан "раван" спектар што указује да је доминантни емисиони механизам термалне природе.